History-Dependent Isotherms and TIRF Calibrations for Homopolymer Adsorption

V. A. Rebar and M. M. Santore*

Department of Chemical Engineering, Lehigh University, Bethlehem, Pennsylvania 18015

Received August 22, 1995; Revised Manuscript Received July 16, 1996[⊗]

ABSTRACT: This work reexamines fundamental issues for the implementation of total internal reflectance fluorescence (TIRF) in quantitative studies of polymer adsorption: the utility of internal calibrations for surface excess and complications stemming from light scattering, chain labeling topography, and quantum yield changes on adsorption. Scattered photons were found to have a greater impact on the signal than documented in the literature, motivating the development of an improved universal calibration. The work then probes the history dependence of TIRF-obtained isotherms for poly(ethylene oxide) (PEO) and (hydroxyethyl)cellulose (HEC) on silica, comparing coverages to those on silica particles. With sufficient equilibration time, the TIRF-obtained isotherm shapes for PEO approached those on silica particles, suggesting linearity of TIRF signal in interfacial chain number. Also apparent for PEO (1 label/chain) was the surface selectivity for high molecular weight populations, which artificially lowered the apparent mass coverage by up to a factor of 2. TIRF-obtained isotherms for HEC were strongly history dependent in a manner that suggested solvent-induced interfacial relaxations and a sensitivity of fluorescein quantum yield to HEC chain configurations.

Introduction

Total internal reflectance (TIRF), also known as evanescent wave induced fluorescence (EWIF), has been used in the biotechnology community to study protein adsorption[1−6] and is recently making its way into the polymer science arena.[7−12] The method is valuable because, in addition to being sensitive to interfacial mass and having adequate time resolution for many adsorption-related processes involving polymers on wetted solids, the method can measure slow interfacial relaxations through the environmental sensitivity of specially selected fluorescent labels and controlled experimental conditions.[13] Also through the use of selective sample preparation, TIRF is capable of interfacial tracer studies[14] and the investigation of specific interfacial populations.[15]

As with all fluorescence methods, certain complications must be addressed quantitatively in order to obtain reliable information from TIRF. First, because the method monitors fluorescent molecules, tags must be chemically attached to the species being studied. Then the possibility that the fluorescent label physically alters the process being studied must be tested. Even without invasive labels, one should interpret fluorescence cautiously. For example, one might intend that a fluorescent label mark a particular species as a simple interfacial assay. Then one must ensure that the fluorescence is linear in concentration and that environmental factors (such as polarity, local mobility, and orientation) do not alter the quantum yield among the samples being compared. In TIRF studies, only a few investigators have attempted to quantify such effects in their particular systems.[1,3,5,12,14]

Aside from label invasiveness and environmental effects, sample heterogeneity and the nature of the fluorescent labeling chemistry must also be considered. With proteins, one molecule is usually identical to the next, although isomeric populations, or "isozymes", may exist. Internally, however, each individual protein molecule is heterogeneous, with acidic, basic, polar, and hydrophobic groups. A randomly labeled protein sample consisting of a single isozyme may therefore contain different populations. For example, in some molecules a label may attach to a polar region, where in other molecules the label may reside in a hydrophobic cleft, and these two proteins may fluoresce differently.

The fluorophore attachment site is less of an issue for homopolymers, since the individual monomers within the chain are identical. Polymer samples can, however, be polydisperse (in molecular weight), a feature which when combined with a particular labeling topology can cause complications. For example, a labeling chemistry placing tags on chain ends will render TIRF studies sensitive to chain number, in contrast to random tag placement, which facilitates measurements of interfacial mass. There is no distinction between these situations for monodisperse samples.

Our implementation of TIRF to study interfacial polymer kinetics on solids immersed in aqueous solutions has thus far employed fluorescein labels.[10−12,15] We previously addressed how the pH sensitivity of this label could be exploited as a probe of interfacial potential in situations where the physics of a poly(ethylene oxide) (PEO) layer adsorbed on silica were nearly constant.[12] The previous work also demonstrated the range of bulk ionic conditions that minimized the variability in the fluorescence from fluorescein labels tethered at an interface. In contrast, this work fixes ionic conditions and explores, as a prerequisite to kinetic studies, the calibrations which translate fluorescence signal to surface excess.

There are several potential means of calibrating the TIRF instrument: the most obvious involves an independent determination of surface excess, for example via radiotracer methods or ellipsometry. Often, independent determinations of coverage require a different sample geometry, for example a particulate substrate or, in the case of ellipsometry, one of high refractive index. This introduces the complication that the adsorption conditions or surface may differ from that in the TIRF experiment, leading to real differences between the TIRF and calibration runs. Therefore, the most appealing methods of calibrating the TIRF instrument are intrinsic methods which rely on the intrinsic TIRF physics.

[⊗] Abstract published in *Advance ACS Abstracts,* August 15, 1996.

S0024-9297(95)01236-8 CCC: $12.00

In this work we closely examine and improve upon internal calibration methods and compare TIRF-obtained isotherms to those generated by an external method on silica particles. This exercise provides two types of perspective: First, one gains insight into the value (and drawbacks) of internal vs independent (silica particle) calibration techniques. Second, one gains insight into different adsorption behaviors on two types of substrates: Any disagreement between the TIRF-generated and external isotherms, going beyond what can reasonably be explained by the assumptions implicit in the internal TIRF calibration, must be considered a real effect. For example, a similarity in shape between particulate and TIRF isotherms indicates that the adsorption behavior is similar on the two surfaces. If the internal and independent calibrations lead to different ultimate levels of coverage but the same isotherm shape, the discrepancy can be explained by fluorescence quenching in the adsorbed layer, not taken into account by the internal calibration. (In such a case the TIRF signal is said to be linear in coverage.) Conversely, if isotherms measured by TIRF differ in shape or history dependence from those found on silica particles, then one can be certain that the adsorption is different in the two situations.

This paper explores issues related to TIRF calibrations and adsorption isotherms primarily from a static perspective. Two polymers, fluorescently end tagged PEO and randomly fluorescently tagged (hydroxyethyl)-cellulose (HEC), are compared on silica surfaces. Two polymers are chosen to highlight which types of features are general and what variations can be driven by a specific polymer chemistry. Of particular importance is the difference in labeling topology. Two silica surfaces are employed: a planar flat surface and spherical silica particles, chosen to provide perspective on the difference between internal and independent calibrations. We show that when sufficient time is allowed for adsorption, PEO adsorption measured via TIRF and independently on silica particles is similar, of a high-affinity form. We also show that HEC exhibits unusual history-dependent effects, probably driven by slow surface relaxations.

The companion paper[16] provides kinetic perspective for FPEO adsorption: Issues of TIRF signal linearity are further clarified and the importance of labeling topology is emphasized.

Experimental Section

Materials. Polymer adsorption on silica was studied in phosphate-buffered saline (PBS, containing 0.147 M NaCl, 0.002 M KH_2PO_4, and 0.008 M Na_2HPO_4). PBS maintained the pH near 7.4, which was essential since fluorescein emissions are highly pH sensitive near pH 6, that of deionized (DI) water.[12] PBS maintains strong interfacial fluorescence and reduces the environmental sensitivity of fluorescein tags during polymer adsorption on silica.[12]

One micron nonporous spherical silica particles (Geltech) comprised a dispersed silica substrate for adsorption isotherm screening tests while acid-washed microscope slides (soda lime glass, Erie Scientific) provided a planar silica surface for TIRF adsorption studies. The microscope slides were soaked in concentrated sulfuric acid for at least 10 h after they had been mounted in the flow cell. Subsequent rinsing with copious amounts of DI water yielded a silica surface,[12,17] and avoiding exposure of the surface to air facilitated reproducible adsorption experiments.

Confirmation of the surface chemistry on slides and particles was obtained by XPS, using a Scienta ESCA-300 high-resolution instrument.[17] For the silica particles, survey spectra revealed an oxygen−silicon ratio of 2.4−2.6, consistent with a silica surface. This ratio was identical for the microscope slides, independent of the surface treatment (cleaning procedure described above). The native microscope slides contained small amounts of sodium, calcium, and potassium (an atomic ratio of 0.08−0.15 each, with respect to silicon), elements which were not present in the silica particles. After treatment with acid, these elements were not apparent in the survey spectra of the microscope slides when measured at glancing (10−15°) take-off angles. Spectra taken at more penetrating angles (80°) on the acid-treated microscope slides showed higher levels of sodium, calcium, and potassium (0.02−0.09 ratio with respect to silicon, for sodium). These observations suggest that acid treatment leaches sodium and other elements from the face of the microscope slide, leaving a silica surface. Analysis of acid-treated slides that had been soaked in the phosphate buffer and then rapidly rinsed in DI water revealed no additional sodium or phosphate, suggesting that these ions do not bind strongly to the adsorbate surface. While the XPS data are instructive in providing information about the microscope slide surface, we are cautious in translating the XPS data directly to the adsorption substrates. Surfaces studied via XPS are exposed to air and then to vacuum, while adsorbate slides in the TIRF cell see subsequent treatment liquids and polymer solutions without exposure to air.

The polymers selected for this study were PEO (MW = 97 400, polydispersity 1.03) from Polymer Laboratories and HEC (Natrosol HR, reported viscosity average MW = 250 000) from Aqualon. The fluorescent label was fluorescein isothiocyanate (FITC), isomer I from Sigma. FITC was covalently bound to the hydroxyl groups on the polymers by reaction at 100 °C for 3−6 h in dibutyltin dilaurate catalyst to which a few drops of pyridine was added. The catalyst was subsequently removed by washing with a nonsolvent for the polymer (tetrahydrofuran for HEC and pentane for PEO). The labeled polymers (FPEO and FHEC) were further purified by dissolving in solvent (toluene for FPEO, dimethyl sulfoxide for FHEC) followed by precipitation with the appropriate nonsolvent. The maximum FPEO labeling density was 1 tag per chain, because PEO chains have hydroxyl groups on only 1 of 2 ends. Individual FHEC batches containing 1.3, 2.7, and 5.3 fluoresceins per chain were prepared. To remove any unattached FITC, the FPEO and FHEC samples were dialyzed against PBS until negligible fluorescence was detected in the dialysate.

A Turner filter fluorometer was employed to assay the fluorescence of the polymer solutions and calibration fluids. This instrument contained a mercury lamp with a broad blue gel filter for excitation near 475 nm, and fluorescence was detected above 540 nm through a sharp-cut high-pass filter (Schott SOG 540).

The PEO molecular weight was measured with gel permeation chromatography (GPC) employing tetrahydrofuran. A Waters instrument equipped with two Ultrastyragel columns (10^3 and 10^4 Å) and a refractive index detector was calibrated with unlabeled molecular weight standard PEO from Polymer Laboratories. Characterization of the FPEO used in this study revealed progressive degradation over its year-long lifetime: Undialyzed FPEO stored dry and in the dark for several months retained its narrow molecular weight character, similar to that of the original PEO from the supplier. During the refrigerated wet storage period following the dialysis, the molecular weight was broadened and reduced by a free radical chain scission mechanism.[18] At the time of this study, the GPC average molecular weight was reduced to near 65K.

Adsorption Isotherms on Silica Particles. Isotherms were generated by adding 0.5 g of dry silica spheres to 7.0 g of fluorescently tagged polymer solution in PBS for each datum. After vigorous mixing by hand, samples were allowed to equilibrate and settle under gravity for 12−24 h. Then the serum was collected and assayed for fluorescence to determine the free polymer concentration. A mass balance yielded the adsorbed amount, and repeating this procedure with polymer solutions of varied concentration yielded adsorption isotherms. For conditions on the plateau of the FPEO isotherm, a second silica charge size, 0.1 g, was attempted and did not significantly affect the isotherm, suggesting that the dispersions were sufficiently dilute. Negligible effects of equilibration time beyond 12 h were found in a previous study.[19]

TIRF Instrumentation. The total internal reflection of a laser beam inside an optically clear substrate produces in the

polymer solution and/or adsorbed layer a standing evanescent wave whose intensity, $I(z)$, decays exponentially normal to the interface.[1−12]

$$I(z) = I_0 e^{-z/\Lambda} \tag{1}$$

The decay length or "penetration depth" of the evanescent wave, Λ, depends on the refractive indices of the substrate, n_g, and polymer solution, n_p, the incident angle inside the glass (θ_g measured from the normal), and the laser's wavelength, λ_0.

$$\Lambda = \frac{\lambda_0}{4\pi\sqrt{n_g^2 \sin^2 \theta_g - n_p^2}} \tag{2}$$

As fluorescently labeled chains adsorb, their labels are excited by the evanescent wave and the fluorescence is measured. In polymer adsorption studies, Λ typically exceeds the adsorbed layer thickness, giving two components to the TIRF signal: from fluorophores on chains in the adsorbed layer and from fluorophores on free chains also in the "evanescent zone".

Our TIRF instrument[10,12,17] employs 488 nm excitation light and detects fluorescence above 540 nm by photon counting. Neutral-density filters attenuate the beam to near 10 μW (spread across surface areas of 3−10 mm^2) to minimize photobleaching. (Separate studies[17] detected no photobleaching over a period of 3 days.) The laser's incident angles is adjusted by a mirror on computer-controlled rotation and translation stages (Aerotech), providing a resolution for θ_g of 0.00085° at the most glancing angles and 0.00102° near transmission. This translates to negligible error in Λ near Λ = 65 nm and a 10 nm error near transmission (for Λ = 900 nm). The laser steering was therefore not the error-limiting element for Λ. The greater error (est. ±0.25° for θ_g) stemmed from alignment reproducibility and the local flatness of the microscope slides.

We employed two black Teflon shear-flow cells following the designs of Lok *et al.*[1] and Shibata and Lenhoff,[6] with thicknesses of 0.5 and 0.4 mm, respectively, but found no impact of channel design on signal level and evolution. The microscope slide substrate comprised one wall of each cell, and to prevent stray reflections from entering the cell, its exterior surface was painted black except for a 9 mm diameter window. The slide was then optically coupled to a waveguide prism with index-matching oil. A Harvard Apparatus syringe pump maintained continuous flow at wall shear rates of 13 and 8 s^{-1} for the 0.4 and 0.5 mm cells, respectively.

TIRF Calibration Procedures. Calibrations translate fluorescence to an adsorbed amount, or for kinetic studies, establish the TIRF signal linearity in the surface excess. Internal TIRF calibrations fall into two categories, angle scanning[7] and concentration based,[3,5] both of which compare the signal from the adsorbed layer to that from nonadsorbed fluorescent molecules in the evanescent zone. The free fluorophores must be distributed uniformly across the cell. Both calibration approaches are potentially susceptible to inaccuracies caused by scattered light reaching dye molecules far from the surface, and both approaches require that the quantum yield of the fluorophore be unaffected by the adsorption process. In this work we evaluate existing measures of scattering and propose an improved approach. The extent to which quantum yield variations affect our results is addressed in the discussion section.

Rondelez's group[7,8] varied Λ (via θ_g in eq 2) from its minimum value to transmission (infinity). The surface excess derives from a Taylor series expansion in $1/\Lambda$:

$$R(\Lambda^{-1}) = \frac{F_{ads}(\Lambda)}{F_{cal}(\Lambda)} = 1 + \frac{\Gamma}{\Lambda C_b} + O\left(\frac{1}{\Lambda^2}\right) \tag{3}$$

Γ is the adsorbed amount, and R is the ratio of F_{ads}, the fluorescence from the layer plus the fluorophores on free chains in the adsorbate solution in the evanescent zone, to F_{cal}, the signal from a nonadsorbing calibration fluid with fluorophores like those on the adsorbate, uniformly distributed throughout the cell (in the absence of the adsorbed layer). The free fluorophore concentration, C_b, is identical in the adsorption and calibration runs. Like the Rondelez group,[20] we experimentally determined the critical angle from the fluorescence intensity and then figured θ_g for other data relative to the critical angle.

This Λ-based calibration may underestimate the adsorbed amount if light, scattered from imperfections in the slide and prism or the polymer solution itself, reaches fluorophores beyond the evanescent zone to increase F_{cal} and F_{ads}. This effect grows with the number of fluorophores on free chains (i.e. bulk polymer concentration and/or cell depth), to the point where all of the scattered photons are adsorbed, the inner filter effect.[3] Further increases in cell depth do not influence the signal. Rondelez corrected for scattering by varying the channel depth and extrapolating to zero depth.[7,8,20]

Fixed-angle concentration-based methods, or "universal calibrations", like those of Hlady *et al.*[3] and Shibata and Lenhoff[5] require the sequential injection of a series of nonadsorbing fluorescent tracers, whose photophysics parallel those of the labels on the adsorbing polymer. In a plot of the fluorescence, F_{cal}, vs concentration, a line is extrapolated from the high-concentration data to the ordinate. Its slope, $A\Lambda$, yields a "universal calibration" for later adsorption experiments:

$$\Gamma = AF_{layer} \tag{4}$$

Here F_{layer} is the fluorescence from an isolated adsorbed polymer layer, in the absence of free chains. Scattering is quantified through the positive y-intercept of the calibration curve and requires that Λ exceed the adsorbed layer thickness by a factor of 4 or more.

Both angle-scanning and concentration-based calibrations require measurements of F_{cal} for a nonadsorbing fluorophore uniformly distributed in the channel without an adsorbed polymer layer. Such experiments, conducted separate from the adsorption experiment, are potentially troublesome. For example, a nonadsorbing calibration fluorophore may be unavailble, or prolonged exposure to solvent might, during the calibration, contaminate the substrate or allow surface regeneration prior to the adsorption run.[21] Also, the use of a new substrate after the calibration may reduce the applicability of the calibration to the adsorption study, since the scattering may vary among flats. We therefore compared the separate calibrations via Rondelez's and Andrade's procedures, to measurements of F_{cal} in the presence of adsorbed polymer layers. Our three methods employed are summarized in Table 1.

Free fluorescein, found not to adsorb appreciably to acid-washed microscope slides,[17] was employed as a calibration agent in "method 1", which parallels Rondelez's and Andrade's procedures. The TIRF signal, F_{cal}, was measured at a variety of Λ from 63 to 3569 nm for buffered fluorescein solutions at concentrations whose filter fluorometer signals were identical to the FPEO solutions employed in adsorption studies. The method 1 calibration runs were conducted independent of adsorption experiments.

FPEO layers were not visibly affected by exposure to dilute fluorescein solutions in PBS.[17] Therefore, in the "method 2" calibration, F_{cal} was determined by subtracting the signal for an FPEO layer contacting PBS from the signal from an FPEO layer contacting a fluorescein solution in PBS. This required two angular scans.

A third method, employing the FPEO adsorbate solution itself as the calibration fluid was attempted. In "method 3", F_{cal} was set equal to the signal from the free FPEO chains in the PBS solution "equilibrating" with an adsorbed layer. This was determined by subtracting the signal of the adsorbed layer in PBS from that of the same layer in contact with the FPEO adsorbate solution, as later shown in Figure 2.

Differences among the three ways to determine F_{cal} for eq 3 deserve comment. While method 1 is most likely to have a uniform fluorophore distribution near the surface, scattering may vary from the calibration run to the adsorption study. Methods 2 and 3 avoid this problem by determining F_{cal} *in situ* during adsorption. An adsorbed layer, however, poten-

Table 1. Methods of Measuring F_{cal}[a]

	calibration fluid	measurement conditions	how
method 1[b]	free fluorescein in PBS	no adsorbed layer present	signal from cell full of fluorescein *minus* signal from cell full of DI water (baseline)
method 2	free fluorescein in PBS	adsorbed layer present	signal from cell full of fluorescein *minus* signal from cell full of PBS (baseline includes layer signal)
method 3	free FPEO in PBS	adsorbed layer present	signal from cell full of FPEO solution *minus* signal from cell full of PBS (baseline includes layer signal)

[a] All measured for a variety of penetration depths. [b] Closely follows Rondelez's method.[7]

Table 2. Different Adsorption Histories Examined

	detail	polymers studied	methods for F_{cal}	analyses employed (eq nos.)
one-shot	single-contact polymer solution on clean surface, includes Λ-scan	FPEO	1, 2, 3	3, 4, 8
sequence 1	sequential introduction of adsorbate solutions, calibration solutions injected between each adsorbate solution, includes Λ-scan	FPEO	1, 2, 3	3, 4, 8
sequence 2	sequential introduction of adsorbate solutions without internal calibration, no Λ-scan	FPEO FHEC	1	3 and constant from eq 8 determined by other histories applied to FHEC

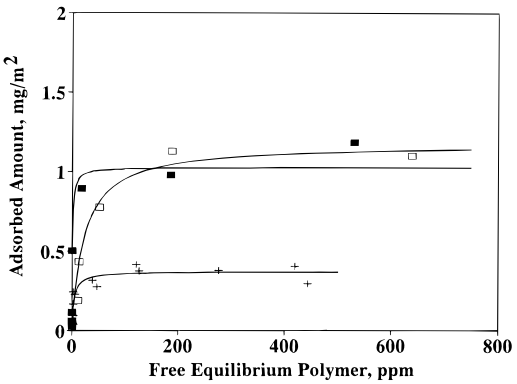

Figure 1. Adsorption isotherms on 1 μm silica beads for FHEC (□) 1.3 labels/chain; (■) 5.3 labels/chain) and FPEO (+) solutions in PBS.

tially perturbs the free fluorophore distribution, a more severe effect for method 3, but one which should diminish as Λ approaches ∞. Angle scan experiments for all three methods were conducted at several FPEO and fluorescein concentrations, facilitating the Λ- and concentration-based calibrations.

TIRF calibrations via methods 2 and 3 required stable adsorbed layers and were conducted only for PEO. For single points on the FPEO isotherm (coined "one-shot" runs), an FPEO solution in PBS was contacted with a clean surface under continuous flow for 40−60 min, usually sufficient for the signal to become level. The laser angle was then scanned to obtain $F_{ads}(\Lambda)$, requiring an additional 15−30 min of contact between the layer and the FPEO solution. Next, continuously flowing PBS was introduced and the angle scan repeated to determine $F_{layer}(\Lambda)$. Flowing deionized (DI) water was then introduced to quench the layer as a check of the baseline,[12] and another angle scan conducted. In several runs, the original FPEO solution was returned to the cell for an additional 3 h of contact, and another angle scan conducted for $F_{ads}(\Lambda)$. Finally, a buffered fluorescein solution, whose fluorescence matched the original polymer solution, was introduced and a final angle scan conducted.

To test the effect of adsorption history, adsorption isotherms were also generated according to a "sequence 1" history: FPEO solutions were introduced into the flow cell in order of increasing concentration from 2 to 500 ppm. Because the internal calibration procedure was time-consuming, it was necessary to reduce the contact time of the solution with the substrate in order to generate an isotherm in a day-long period. Therefore, only the first 2 ppm solution contacted the surface for 70−90 min including angle scanning (sometimes done twice). Then following the series of DI water, PBS, and fluorescein solutions with their angle scans described above, the next polymer adsorbate solution was introduced. The incubation times prior to data acquisition for the subsequent polymer solutions were shorter (10−15 min), but still of sufficient length such that the signal appeared steady before angle scans were made. With 0.5 h long angle scans, the total incubation time for each solution was 45 min.

Since FHEC layers were unstable in solvent flow, the internal calibration methods 2 and 3 could not be applied. Therefore, *ex situ* calibrations (method 1, and an improved universal calibration, described below) were employed. FHEC adsorption was studied sequentially, according to a "sequence 2" history, without *in situ* measurement of F_{cal}: Solutions were introduced sequentially with 30−45 min polymer incubation periods of continuous flow followed by 30−45 min solvent flushes. These runs were conducted at a fixed angle of 63 or 66 nm. The sequence 2 procedure was duplicated for FPEO adsorption for comparison to FHEC behavior. The different types of adsorption histories are summarized in Table 2.

Results

General FPEO and FHEC Behavior. Figure 1 illustrates the general features of FPEO and FHEC adsorption on silica particles. Both polymers display steep initial slopes and, above free polymer concentrations of 100 ppm, flat plateaus. The ultimate FHEC plateau coverage (1.1 mg/m^2) is consistent with the literature;[22] however, the FPEO plateau coverage (0.4 mg/m^2) is at the low end of that reported.[23−26] In the literature, most of the PEO adsorption was from DI water, and reflectivity experiments in our laboratory indicate slightly lower coverage in PBS.[17,27] The flat plateau region for FPEO is a feature later seen in TIRF adsorption studies.

Two FHEC labeling densities, 1.3 and 5.3 per chain, negligibly affect the plateau coverage, although the initial slope is steeper for the more densely labeled sample. It remains unclear if such detail is within experimental error. The impact of fluorescein tagging on FPEO adsorption was previously explored by comparing mixtures of labeled and unlabeled populations with samples where all the chains were labeled.[11] No impact of labeling was found for PEO (100 000, polydisperse) adsorption on silica particles. For the FPEO samples employed in this work, the surface selectivity for long chains far outweighed any effect of fluorescein−surface interactions on the polymer partitioning between the surface and the solution.[17]

Perspective into the TIRF method is provided in Figure 2 by adsorption traces (Λ = 66 nm) for bulk FPEO and FHEC (2.7 labels/chain) solutions on the isotherm plateau (200 ppm). The baseline is recorded,

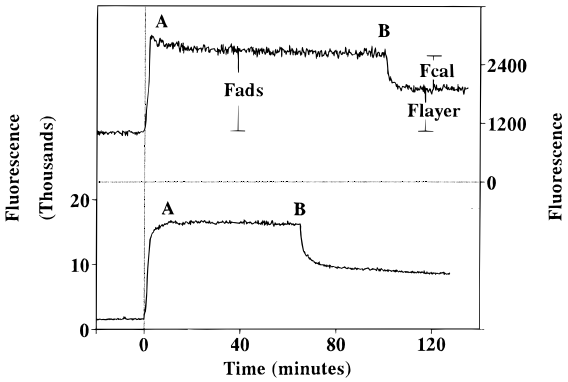

Figure 2. Adsorption kinetics for 200 ppm solutions of FPEO (above) and FHEC (below) for a wall shear rate of 8 s^{-1}.

and the clock started when flowing polymer solution (8 s^{-1} wall shear rate) in PBS is introduced. The signals rise as adsorption proceeds, and at points A turn over as the surfaces saturate. In the FPEO run an overshoot occurs before the signal becomes level. By 40−60 min, the incubation period for one-shot run calibrations via methods 2 and 3, the signal (F_{ads}) is fairly level. Finally, at B, PBS is reinjected and free chains are removed from the evanescent zone, leaving the signal due exclusively to the adsorbed layer, F_{layer}. At times sufficiently longer than that for PBS reintroduction (cell filling takes ∼1.3 min), the FPEO layer appears stable while the FHEC signal decreases. In Figure 2, angle scans were eliminated to highlight kinetic features; however, F_{cal}, F_{ads}, and F_{layer} for method 3 and $\Lambda = 66$ nm are illustrated.

Quantification of the TIRF Signal. Equations 3 and 4 were initially employed to quantify the FPEO surface excess in one-shot and sequence 1 runs. Examples for the Λ and concentration dependence of F_{cal} determined via methods 1−3 are shown in Figure 3. Figure 3A for method 1 illustrates F_{cal} for fluorescein in PBS flowing through the TIRF chamber, without adsorbed polymer. The fluorescein concentration is reported in equivalent FPEO concentration units, meaning that the fluorescein solution in question had the same filter fluorometer signal as an FPEO solution with the concentration indicated. The TIRF signal in Figure 3B for method 2 resulted from a similar series of fluorescein solutions, each in the presence of adsorbed FPEO (although the layer's fluorescence is not included in F_{cal}). Figure 3C for method 3 shows the TIRF signal attributed to fluorophores on free chains for a series of FPEO solutions, each measured in the presence of their respective adsorbed layers. The data in Figures 3B and 3C were obtained during one-shot adsorption runs.

Figures 3B and 3C for calibration methods 2 and 3, respectively, are nearly identical as expected: Fluorescein and FPEO solution pairs having the same externally determined solution fluorescence were measured in the presence of the same adsorbed layer. The particular method 1 data in Figure 3A are less intense than analogous calibration data obtained via methods 2 and 3. For all the one-shot and sequence 1 runs, methods 2 and 3 were generally in good agreement while the method 1 calibrations sometimes showed a stronger and sometimes weaker fluorescence than methods 2 and 3. Such variability may have arisen from slight differences in cell assembly, alignment, and scattering between method 1 calibrations and adsorption runs.

In Figure 3 the free fluorophore contribution to the TIRF signal increases with concentration for all Λ. More important, calibrations pass through the origin

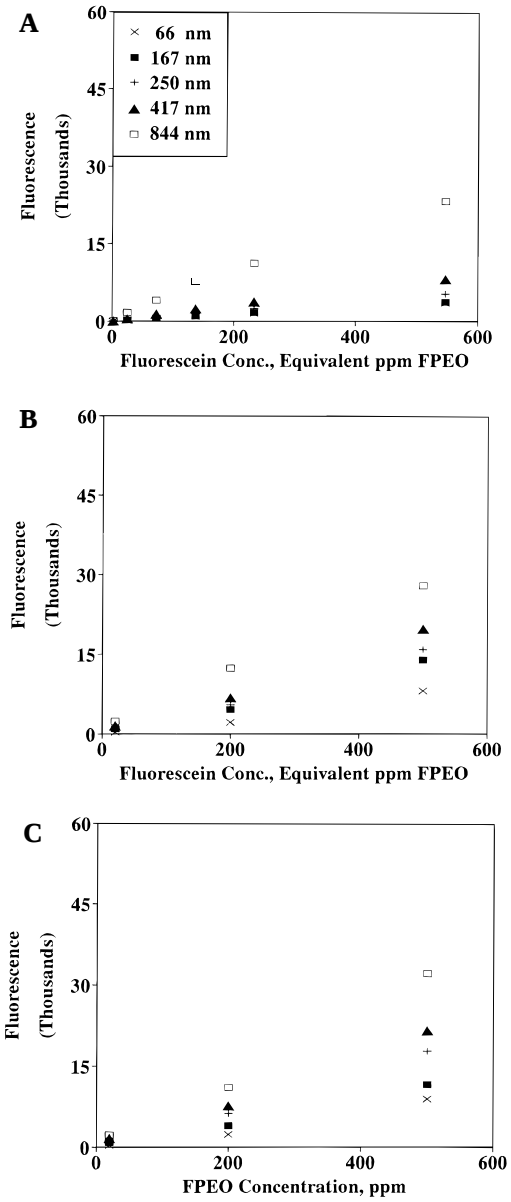

Figure 3. TIRF calibration curves at different penetration depths, employing three calibration methods (in Table 1). (A) Method 1: FITC in PBS with no adsorbed layer present; (B) method 2: fluorescein in PBS in the presence of an adsorbed layer; (C) method 3: FPEO in PBS in the presence of an adsorbed layer. (For data taken in the presence of an adsorbed layer, the layer fluorescence in not included in the ordinate.)

and are nearly linear, not concave down. The lack of a positive y intercept suggests minimal scattering;[3,5] however, run−run variations in F_{cal}, for example the difference between the data in Figures 3A and 3B, indicate otherwise. The slopes of the lines in Figure 3, when used in the universal calibration per eq 4, gave adsorbed amounts more than an order of magnitude below expectations, also suggesting significant scattering. A second test, increasing the cell depth from 0.5 to 1.5 mm, revealed scattered light: For $\Lambda = 66$ nm, the increased cell depth led on average to a 90% increase in F_{cal} (via method 3). Scattering was always present but varied in magnitude among runs which involved cell reassembly. The run−run variation in the cell depth experiment confounded Rondelez's scattering correction,[7] which extrapolated to zero cell depth.

It was enlightening to exploit the Λ dependence of the free fluorophore signal to quantify the scattering contribution to F_{cal} and, ultimately, to arrive at an "improved" universal calibration, different from An-

drade's concentration-based approach which relied on the inner filter effect.[3] Both our and Andrade's approaches involve the optical physics of TIRF:[7]

$$F = K(\Lambda)\int_0^\infty c(z)\mathrm{e}^{-z/\Lambda}\,\mathrm{d}z \tag{5}$$

The fluorescence, F, is a function of optical geometry, laser intensity, and quantum yield, via a lumped proportionality constant, $K(\Lambda)$. In eq 5, the fluorescence is the convolution of the evanescent field intensity from eq 1 with the fluorophore concentration profile $c(z)$. For uniformly distributed fluorophores, without scattering and without an adsorbed layer, the signal should be first order in Λ, but the linearity is confounded by the Λ dependence of K:

$$F_{\mathrm{cal}} = K(\Lambda)C_{\mathrm{b}}\Lambda \tag{6}$$

For fluorophores right at the interface, a delta function integration of eq 5 leads to

$$F_{\mathrm{layer}} = \Gamma K(\Lambda) \tag{7}$$

Here it becomes clear that the lumped constant $K(\Lambda)$ is the inverse of the universal calibration in eq 4. The signal from the adsorbed layer in contact with solvent can be employed to normalize eq 6 to remove the Λ-dependent optical constant:

$$\frac{F_{\mathrm{cal}}}{F_{\mathrm{layer}}} = \frac{\Lambda C_{\mathrm{b}}}{\Gamma} \tag{8}$$

A graph of $F_{\mathrm{cal}}/F_{\mathrm{layer}}$ vs Λ will provide, in addition to a measure of the scattering (via deviations from eq 8), the surface excess.

Figure 4A shows method 3 data for two one-shot runs and the 200 ppm injection from a sequence 1 run represented according to eq 8. Each data set is nearly linear in Λ, with the same slope resulting from multiple runs at a particular concentration (corresponding to surface excesses of 0.07 and 0.06 mg/m^2 for 200 and 500 ppm solutions, respectively). In contrast to the predictions of eq 8, the y intercepts are positive and exhibit run−run variations. The data at $\Lambda = 66$ nm deviate positively from linearity. Both the overall positive y intercept and the positive deviation of the data at small Λ are attributed to scattering, which is a strong function of Λ at small Λ but goes more nearly constant at moderate values of Λ, less than transmission.

Figure 4A also contains dashed lines parallel to the data for 200 and 500 ppm FPEO concentrations, but passing through the origin. These dashed lines show the "evanescent" portion of the signal per eq 8. The vertical distance between each datum and the dashed line of the appropriate concentration represents the fluorescence from scattering for that datum. The fraction of the signal from scattering for each data set in Figure 4A is shown in Figure 4B. This scattering component of the signal decreases as Λ increases, because as $\Lambda \rightarrow \infty$, the scattering fraction is nearly constant but the evanescent signal diverges. Analyses like those in Figure 4 were repeated for one-shot and sequence 1 FPEO data and for all three methods by which F_{cal} was obtained. Measurements of F_{cal} via method 1 differed from methods 2 and 3 by 40% as a worst case, while all data for methods 2 and 3 were self-consistent.

Obtaining surface coverages via eq 8 is equivalent to Rondelez's approach, so plotting data according to eq 3

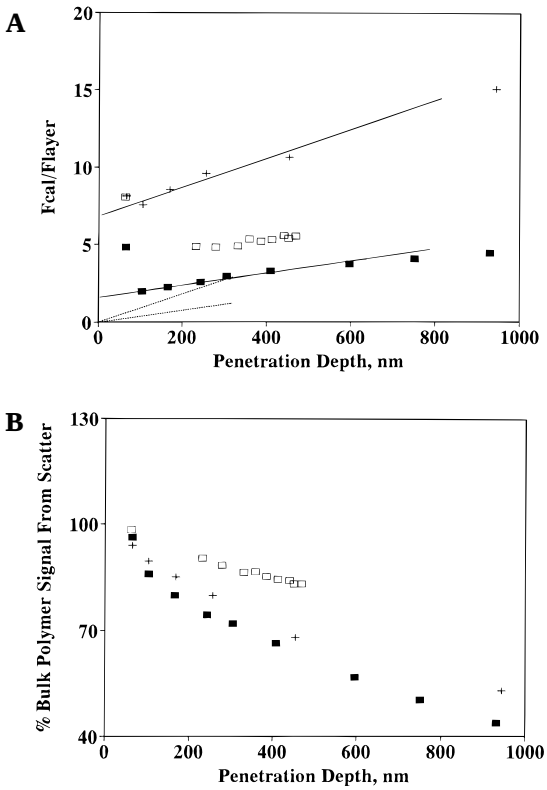

Figure 4. (A) Penetration depth dependence of the signal from free FPEO (F_{cal}, method 3) normalized on that of the appropriate adsorbed FPEO layer (F_{layer}) for bulk concentrations of (■) 200 ppm single-shot run, (+) 500 ppm single-shot run, and (□) a 200 ppm datum from a sequence 1 run. Dashed lines run parallel to the data, passing through the origin. (B) Fraction of the free signal attributed to the scattering for the cases shown in (A).

in Figure 5 provides additional insight. Here R versus $1/\Lambda$ is shown for one-shot FPEO runs at 20 and 200 ppm (the latter from Figure 4). Data for all three methods of obtaining F_{cal} are included. In Figure 5A, the ratio $R = F_{\mathrm{ads}}/F_{\mathrm{cal}}$ is not corrected for scattering. In Figure 5B, the scattering contribution is quantified as in Figure 4B and subtracted from F_{ads} and F_{cal} prior to calculating their ratio. In Figure 5A the y intercepts for methods 2 and 3 approach unity, in accord with eq 3; however, the y intercepts for method 1 deviate slightly. The magnitude of R for the 20 ppm run exceeds that for the 200 ppm run because, per eq 3, R is inversely proportional to the bulk concentration. All data sets in Figure 5A become flat as $1/\Lambda$ increases, in opposition to expectations,[7,8] and the right-most datum in each set (for $\Lambda = 66$ nm) is below that for the preceding datum ($\Lambda = 104$ nm). The surface coverages obtained from the limiting slopes per eq 3 (0.016 mg/m^2 for the 20 ppm FPEO solution and 0.024 mg/m^2 for the 200 ppm solution) are far below expectations for PEO adsorption[21−24] and the results in Figure 1. All these problems can be explained by an artificially high value of F_{cal} due to scattering, with the greater scattering found at smaller penetration depths. With F_{cal} and F_{ads} corrected for scattering, the resulting linearity in Figure 5B is more satisfactory. Coverages are 0.06 mg/m^2 for the 20 ppm FPEO solution and 0.07 mg/m^2 for the 200 ppm solution.

The Λ-scanning analysis is easily applied to layers such as FPEO that are resistant to solvent washing; however, the procedure to obtain all the necessary data is cumbersome and may not be workable when transients are rapid. Also, adsorption from a very dilute solution may not give sufficient signal to quantify F_{cal}-

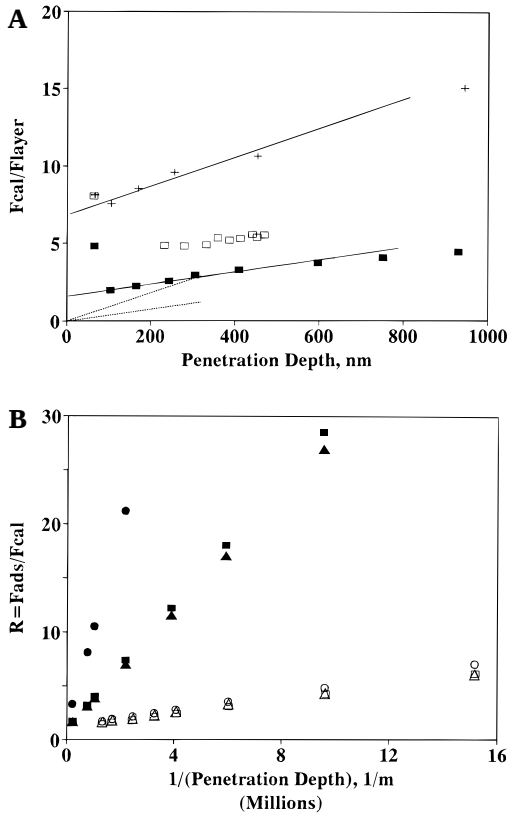

Figure 5. Ratio plot analysis, via eq 3, of two FPEO one-shot adsorption runs following a 4 h incubation period for bulk solution concentrations of 20 (solid symbols) and 200 ppm (hollow symbols). The calibration fluids follow method 1 (●,○), method 2 (▲,△), and method 3 (■,□). (A) Data uncorrected for scattering; (B) data with scattering effects subtracted.

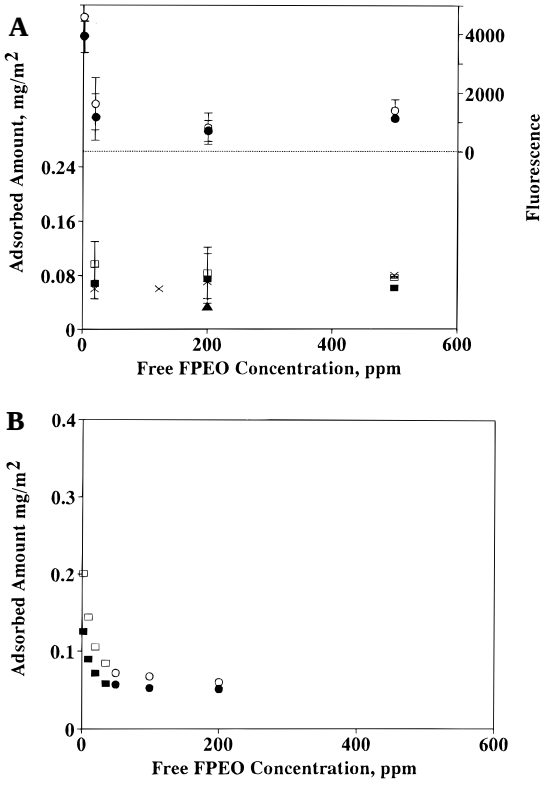

Figure 6. (A) Above (right ordinate): (○,●) raw fluorescence signal at 1 and 4 h incubation time and $\Lambda = 66$ nm from each adsorbed FPEO layer in one-shot experiments in the absence of free chains. Below (left ordinate): Amount of adsorbed FPEO: (×) sequence 1 runs; (□) single-shot data for 1 h incubation period; (■) single-shot data for 4 h incubation period; (▲) single-shot data employing mixture with 25% labeled chains. (B) Adsorbed amount of FPEO in sequence 2 runs calculated based on universal calibration. Alternating 45 min polymer solution and PBS contact periods, with polymer solution increasing order, within each set, as shown.

(Λ). An improved universal calibration relying on angle scanning (as opposed to the inner filter effect) can be obtained from several runs on the isotherm plateau and analysis via eq 8 to yield plots like Figure 4A. On the plateau of the isotherm, where the surface excess is constant, the slopes should be linear in the bulk concentration, which was indeed the case. Then the universal calibration factor $K(\Lambda)$ can be algebraically determined from eq 6 or 7. From an average of many single-shot and sequence 1 runs, $K(\Lambda{=}66\text{ nm})$ was 3161 and 3200 m^2/mg for methods 2 and 3, respectively, but was 1875 m^2/mg via method 1. This improved Λ-based universal calibration was employed to determine adsorption isotherms for the relatively less stable FHEC layers and FPEO layers at short incubation times.

Adsorption Isotherms from TIRF. Figure 6A shows scattering-corrected TIRF-obtained isotherms for FPEO for one-shot runs with bulk concentrations of 20, 200, and 500 ppm and FPEO incubation times of 1 and 4 h prior to Λ-scanning. The points represent averages of several runs, and the error bars show the 95% confidence limit. Data from a sequence 1 adsorption run with FPEO are also included, for bulk concentrations of 2, 20, 123, 200, and 493 ppm. The adsorbed amount for the 2 ppm injection is not shown because F_{cal} (at 2 ppm) was too weak to be accurately measured via methods 2 and 3; however, the total incubation period with the 2 ppm solution was ∼90 min prior to the introduction of the other solutions. Also shown in Figure 6A is a one-shot datum for an FPEO mixture with an overall concentration of 200 ppm and containing 25% labeled FPEO chains and 75% unlabeled PEO. All surface excesses were quantified by examining the Λ dependence of F_{cal}, F_{layer}, and F_{ads} per Figure 4 and eq 8 with F_{cal} obtained via method 3. For the one-shot runs with 1 and 4 h incubation periods, the raw fluorescence intensities (on the right axis at the top of Figure 6A) of the adsorbed layers (F_{layer}) with $\Lambda = 66$ nm are also shown, with the 2 ppm datum included.

The surface excesses measured for the one-shot and sequential procedures were similar, with the mixture data yielding slightly lower coverages for reasons to be discussed. Like the adsorption on silica particles in Figure 1, the isotherm plateau in Figure 6A is relatively flat; however, the TIRF-obtained coverages are lower than those on the particles. The sequence 1 runs gave the flattest plateaus while the one-shot data measured at 1 h yield a slightly decreasing coverage with increasing bulk FPEO concentration. Also apparent is a slight reduction in coverage with increased incubation time, most pronounced for the most dilute adsorbate solutions (20 ppm). The fluorescence from an adsorbed layer measured at $\Lambda = 66$ nm was proportional to the coverage obtained via the formal calibrations. This suggested that the universal calibration could be broadly applied, as Λ significantly exceeded the FPEO layer thickness.

Figure 6B illustrates sequence 2 isotherms, with quantification of the adsorbed amount via the improved universal calibration at 66 nm. Here FPEO solutions and PBS have incubated alternately with the surface, each for 45 min. In two data sets, FPEO solutions are introduced in increasing order of concentration: 2, 10, 20, 35, and 50 ppm, with PBS in between each. In the third and fourth data sets the polymer solutions are

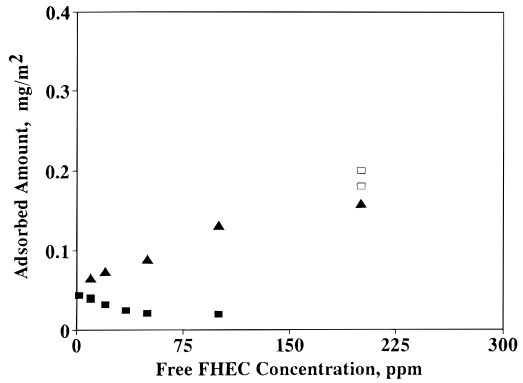

Figure 7. Adsorbed amount of FHEC in sequence 2 runs, calculated based on universal calibration: (■) introduced in order of increasing concentration with alternating 40 min contact periods of PBS and polymer solution; (▲) introduced in order of decreasing concentration with alternating 30 min contact periods of PBS and polymer solution; (□) single data with 10 and 60 min polymer incubation period, 2 min PBS contact period.

introduced in order of increasing polymer concentration: 50, 100, and 200 ppm, also with PBS between each. As the bulk concentration is increased from the most dilute concentration (2 ppm), the apparent coverage decreases markedly. At higher concentrations approaching the isotherm plateau, the bulk polymer concentration appears not to affect the coverage. Figures 6A and 6B together suggest decreased coverage with incubation time, especially for dilute bulk polymer solutions, and long-time behavior parallel to the coverage on silica particles.

The TIRF-obtained isotherms for FHEC in Figure 7 were determined via the improved universal calibration from the FPEO data (methods 2 and 3), accounting for the difference in the labeling densities of the FPEO and FHEC. The coverage levels in Figure 7 are about a factor of 5−6 times below those on the silica particles (Figure 1) when solutions of high concentration are introduced first. History-dependent behavior is evident: Introduction of dilute solutions followed by more concentrated ones yields coverages far below expectations, and the coverages become progressively lower as the runs proceed, in opposition to expectations. The apparent coverage also decreases when concentrated solutions are followed by more dilute ones. We generally observed that the coverages were insensitive to the incubation time with FHEC solutions, but strongly dependent on the time in which layers contacted flowing PBS.[17]

Discussion

Calibration Methods. The intent of this work was to establish an internal calibration of the TIRF instrument and to compare TIRF-obtained isotherms for FPEO and FHEC to those on silica particles. Previous concentration-based[3] and Λ-based[7] TIRF calibrations employed separate runs for calibration and adsorption, potentially leading to inaccuracies if scattered light made variable contributions to F_{cal}. This work therefore compared F_{cal} values measured separate from adsorption experiments (method 1) to those made *in situ* during adsorption (methods 2 and 3).

As anticipated, the *in situ* calibrations were superior to those via method 1, in terms of a smaller run−run variation in the calibration constant; however, several points must be emphasized. First, *in situ* methods require that layers be resistant to solvent washing, as indicated in Figure 2 for FPEO. Second, with *in situ* calibrations care must still be taken to quantify the contributions of scattered light:[17] An influence of cell depth on F_{cal}[17] revealed a significant amount of scattered light despite a linear dependence of F_{cal} on concentration in Figure 3. Therefore, scattering contributions may generally be greater than evident from the inner filter effect[3−5] if the amount of scattered light approaches the evanescent wave intensity. In contrast, previous fixed-angle concentration-based calibrations,[3−5] relying on the inner filter effect, required that scattering be a small contribution to the signal. Scattered light confounds calibration via eq 3 through deviations of the R vs $1/\Lambda$ plot (Figure 5A) from the expected linear relationship (eq 3), even for the *in situ* calibration. The onset of the deviation from linearity occurred at large penetration depths, suggesting the adsorbed layers were on the order of 500 nm thick, an impossibility for FPEO with its molecular weight less than 100K and coverages on the order of 0.4−1.0 mg/m^2.[23]

Our improved analysis approach, which relies on both the concentration and Λ dependence of F_{cal}, is more robust than the previous calibration methods for systems suffering from more intense scattering, and because it does not require repeat runs with different cell depths, it is easier to apply than Rondelez's scattering correction. It also appears that plotting data as a function of Λ as opposed to $1/\Lambda$ tends to magnify error less, as data plotted according to eq 8 (Figure 4A) were more nearly linear with a reasonable slope (and less guesswork in choosing a slope) than the same data plotted via eq 3 (Figure 5A).

Our Λ-based method to isolate scattering is not without potential complications. Equation 8 specifies that F_{cal}/F_{layer} be linear in Λ and pass through the origin. It is not immediately clear, however, what line (dashed) through the origin should be chosen to represent a particular concentration in plots such as Figure 4A. The only requirement is that the data must lie on or above the line because scattering artificially increases F_{cal}. That it is acceptable to apply the slopes from the data as we did is supported by two findings: First, for repeat runs at a fixed bulk concentration, similar slopes were obtained, but day-to-day variations resulted in different y intercepts. Also, for bulk concentrations corresponding to the isotherm plateau (Γ fixed), the slopes were proportional to the bulk concentration, in accord with eq 8. Of course, it would be possible to choose dashed lines of lesser slope, still leaving all the data above the dashed line and maintaining the proportionality to C_b. Our $K(\Lambda)$ values therefore estimate the minimum scattering and may slightly underpredict Γ.

The universal calibration of eq 4 requires that Λ significantly exceed the adsorbed layer thickness, an assumption also implicit in our treatment since eq 7 was obtained by placing all the fluorophores at $z = 0$. The universal constant $K(\Lambda)$ in eq 7 yields errors near 10% when the Λ is within 4 times the adsorbed layer thickness. Indeed, the universal calibration may underestimate the coverage of the thicker[22] FHEC layers. The proportionality, in Figure 6A, between the coverage determined from the Λ dependence and the signal from the adsorbed layer for $\Lambda = 66$ nm (and generally observed by us)[10,11] argues that the universal calibration is valid at 66 nm for FPEO layers. This also means that the upturn of the 66 nm ratio in Figure 4A and the downturn of the 66 nm R value in Figure 5A is due to greater scattering at 66 nm. The scattering contribution at small Λ is highly variable because large angular displacements of the laser (large differences in beam path) yield moderate changes in Λ. Toward transmis-

sion, the laser is only slightly repositioned, hardly altering the scattering but significantly affecting Λ.

Adsorption Isotherms: TIRF vs Silica Particles. Two primary differences were apparent between isotherms measured by TIRF and those on silica particles. First, coverages measured by TIRF were significantly lower than those on particles for both FPEO and FHEC. Second, a time dependence was apparent in TIRF-measured isotherms: Any history-dependent adsorption behavior on the silica particles cannot be resolved because of the time associated with gravity-driven sedimentation. The particulate isotherms represent the limiting long incubation time surface coverage.

The most obvious explanation for the low coverages measured by TIRF is that the planar and particulate substrates were different. One possible difference between the two surfaces is roughness. A higher coverage (based on apparent macroscopic area) should be found on the rougher of the two chemically similar surfaces because on rough surfaces there is a greater available adsorption area per unit of apparent macroscopic area. Therefore, a greater roughness on the silica particles than on the flats would explain the relative coverages we observe. The silica particles, however, appear smooth and spherical in our SEM micrographs[17] and are reported by GelTech to be nonporous in nitrogen BET studies. Indeed the nitrogen BET areas from GelTech concurred with our calculations based on sphere diameter (2.7 m^2/g). Also, AFM studies of the microscope slides revealed an rms roughness of 4 nm, with most features smaller or the same size as the polymer coils, such that the microscopic area available for adsorption and the apparent macroscopic area were the same order of magnitude. Therefore, differences in the true adsorption areas cannot explain the very low coverages measured by TIRF.

Differences in surface chemistry can also cause differences in polymer adsorption. While XPS studies of both substrates revealed silica, we appreciate that the state of the surface oxygens will significantly affect the affinity for adsorbing polymer. While the SiO_2 particles were used as supplied, the planar surfaces for TIRF were acid treated to improve their affinity for PEO. (Studies in our laboratory[17] show that the acid-treated silica does indeed adsorb more FPEO than untreated silica.) Our understanding of the surface chemistry therefore suggests that the coverage on acid-treated flats should be at least as high as that on silica particles.

Desorption of loosely bound chains can potentially lower the coverages measured via TIRF. Loosely bound chains, if they desorb rapidly upon introduction of PBS, would artificially elevate F_{cal} and detract from F_{layer}. The similarity of F_{cal} values from methods 2 (free fluorescein) and 3 (FPEO adsorbate), in Figure 3, suggests only a small contribution of loosely bound chains to F_{cal}. Desorption of 90% of the originally adsorbed chains is required to explain coverages of $\sim$0.1 mg/m^2 when those near 1 mg/m^2 are expected. The signal drop upon PBS introduction was usually too small to be associated with desorption of more than one-half the originally adsorbed chains. Hence, it is unlikely that the desorption of loosely bound chains contributes significantly to inaccuracies in internal TIRF calibrations for FPEO adsorption.

Preferential adsorption of unlabeled chains, if it occurs, will also cause TIRF-obtained coverages, based on internal calibrations, to err on the low side. We previously tested FPEO for preferential adsorption by generating isotherms on silica particles for mixtures of labeled and unlabeled chains.[11,19] These studies, where both labeled and unlabeled chains were polydisperse near 100 000 molecular weight, revealed no statistically significant trends in favor of preferential adsorption. Preferential adsorption for unlabeled FHEC chains was determined to be minimal in Figure 1B, where the density of labels on the HEC is varied.

In cases where chains are labeled on their ends, it is possible that the preference of the surface for high molecular weight populations within a polydisperse sample will act to lower the density of labels on adsorbed chains relative to those in solution. This concept derives from the fact that for polymers of moderately high molecular weight, adsorption of high molecular weight chains is greatly favored in competitive situations, but molecular weight has only a secondary effect on the total surface coverage.[26] For a given adsorbed mass, layers containing higher molecular weight chains contain fewer ends than layers of lower molecular weight. GPC analysis of FPEO solutions showed that, after contact with silica particles, the supernatant was depleted of the high molecular weight half of its chains.[17] This means that molecular weight competition is significant for FPEO. In contrast, the fluorescence from an adsorbed layer of randomly labeled FHEC will not reflect molecular weight driven competition.

For FPEO, the molecular weight selectivity may cause the TIRF-measured coverage to be underestimated by a factor of 2. Recall that the FPEO was originally monodisperse, with a molecular weight of 97K, but became polydisperse through a free radical chain degradation which attacks the chain at random points.[18] For a GPC-average molecular weight near 65K, each original chain may be "cut" at least once. Therefore there will be a small population of long chains approaching the original chain length, but whose fluorophores have been "cut off" with the bond breakage on the PEO chain near the label. There will also be an equal population of long chains which have lost a small piece of their unlabeled end. These two long populations will be preferred on the surface, such that the surface will contain 1 label for every 194K of adsorbed polymer backbone. The free solution, which is continuously replenished, however, will contain 1 label for every 97K of backbone, regardless of the sample degradation. Therefore, as the surface approaches equilibrium, the internal calibration will underestimate the FPEO coverage by a factor of 2 because the calibration fluid is labeled half as much as the adsorbed chains. A similar effect in the particulate FPEO isotherms may explain why the observed plateau coverage of 0.3 mg/m^2 was low compared with values in the literature (0.7$-$1.5 mg/m^2), while the FHEC coverage measured on silica particles concurred with the literature.

Differences in the labeling density within the layer and in the solution cannot fully explain the order of magnitude in the disparity between the coverage levels observed for FPEO on silica flats and particles. A reduction in the quantum yield of the fluorophore in the adsorbed FPEO and FHEC layers, discussed in the next section, is the most likely reason why coverages obtained by internal TIRF calibrations were an order of magnitude below expectations.

The influence of adsorption history on the FPEO and FHEC isotherms is of note. For FPEO, one-shot and sequential adsorption histories gave coverages all of which converged (at long incubation times) to the same level, 0.06$-$0.07 mg/m^2, if one believes the internal calibrations. This same isotherm shape, characteristic of high-affinity adsorption, was also seen previously on the silica particles: a flat broad plateau extending to

concentrations as low as 2 ppm. The steep initial isotherm rise occurs below concentrations employed in this study. The counterintuitive isotherm shape in Figure 6B for sequence 2 FPEO adsorption stems from the reduced incubation times (45 min) at low concentrations for this particular history. The top of Figure 6A indicates that for FPEO solutions of 2 ppm, the layer fluorescence evolves very slowly, beyond 4 h contact time. We show in the companion paper[16] that the fluorescence approaches a level similar to that found for higher concentrations only after 8 or more hours.

For FPEO, the injection history of the adsorbate solutions had little effect on the ultimate coverage, so long as sufficient incubation time in the adsorbate was achieved. Both one-shot and sequential adsorption histories showed that the coverage actually appears to decrease as the incubation in the adsorbate solution proceeded. The next paper in this series[16] argues that the competition between high and low molecular weight populations is the most likely reason for for signal drop with increased incubation time. It is shown that the mass transfer limited nature of exchange between long and short chains is the reason why the incubation time effect is very pronounced for the most dilute solutions, as indicated in Figure 6. Notably this trend is not expected and was not observed for FHEC, which is randomly labeled.

The time-dependent effects found for FHEC were markedly different from those exhibited by FPEO. For FPEO, the TIRF signal decreased with increased time in the adsorbate solution, while for FHEC the contact time with the adsorbate solution had no effect beyond the first 10 min (as shown for data at 200 ppm in Figure 7). In contrast, incubation in PBS had no visible effect on FPEO layers while FHEC layers were sensitive to PBS exposure. For FHEC, the signal decreased with increased PBS contact, even if the layer was exposed to more concentrated FHEC solutions late in the run (Figure 7). This history dependence caused a disparity of the FHEC isotherm shapes, measured by TIRF in increasing and decreasing order of concentration, both of which differ from those measured on silica particles. This is most important, for we did not observe convergence of the coverage to a single level (for each free concentration attempted). These observations suggest that FHEC layers experience relaxations causing desorption of some of the originally adsorbed chains or slow reductions in the fluorescein quantum yield.

Quenching. It was argued earlier that, without significant chemical and topological differences between flat silica and particle surfaces, the low coverage seen via TIRF should be attributed to a reduction of the fluorescein quantum yield upon polymer adsorption. The potential for quenching is the primary drawback of all internal TIRF calibration methods. In order to assess the extent of quenching, one needs an independent measure of the coverage. The previous arguments in favor of quenching, based on the silica particle reference coverage and based entirely on static considerations, are not as convincing as arguments stemming from kinetic considerations which provide an independent estimate of coverage in the TIRF studies for FPEO.

We estimate, based on the following kinetic features, that the actual FPEO coverage in the TIRF studies was 0.7−0.8 mg/m^2, in agreement with the literature.[21−24] The key to the estimated coverages derives from the evidence that FPEO adsorption is transport limited: For FPEO adsorption runs on bare surfaces, we observed a near-linear rise in the TIRF signal with time, like that shown in Figure 2. The initial slope was proportional to the bulk concentration and scaled approximately as wall shear rate to the one-third power.[17] For mass transport limited adsorption, the coverage increases linearly with time, up to the point where the surface is nearly saturated, or when surface crowding hinders the further adsorption. Dijt *et al.*[20,23] have shown by reflectivity that for PEO, mass transport limited adsorption can persist up to 80% or more of the equilibrium coverage. By a flow tracer method,[11,16] we have independently determined the free chain diffusivity of the FPEO in this work to be 3×10^{-7} cm^2/s. Using this value of the diffusivity in the Leveque approximation for mass transport limited adsorption rates, we found that the linear portion of the signal rise during FPEO adsorptions persisted for times sufficient to yield coverages of 0.7−0.8 mg/m^2. This coverage level is in qualitative agreement with the coverages measured on silica particles, since the fluorescence-based mass balance used to determine the coverage on the particles is susceptible to the molecular weight driven reduction in the labeling density of adsorbed chains. If the FPEO coverages reported on the particles in Figure 1 were low by a factor of 2 (a factor consistent with GPC analysis of the supernatant[17]), then the plateau coverage on the particles would be just above 0.6 mg/m^2, while that on the silica flats would be 0.7−0.8 mg/m^2, good agreement when one accounts for small differences in surface chemistry and roughness.

With actual FPEO coverage levels of approximately 0.75 mg/m^2 and coverages from the internal TIRF calibration of 0.065 mg/m^2 (for long incubation periods), we estimate that quenching accounts for approximately a factor of 5 error in the calibration. Another factor of 2 error in the calibration likely stems from changes in the labeling density of the adsorbed layer due to molecular weight driven exchange. Notably, the highest coverages (based on the internal calibration) seen for FPEO adsorption corresponded to times sufficient for surface saturation but insufficient for significant chain exchange. This maximum coverage level, for the low concentrations in Figure 6B, is approximately a factor of 5 below the coverage calculated from kinetic considerations.

The assessment of quenching for FHEC is more difficult to carry out because of the nonconvergent history dependence of the FHEC isotherms. Kinetic arguments do, however, favor significant quenching in FHEC layers. Based on the wall shear rate sensitivity of the initial fluorescence rise, we concluded that FHEC adsorption was also wall shear rate limited.[17] The time scales associated with FHEC adsorption are consistent with plateau coverages on the order of 1 mg/m^2, in qualitative agreement with the isotherms on the silica particles. (We have not extracted a diffusivity for FHEC and therefore cannot be as quantitative in our analysis as we had for FPEO.) The silica particle isotherms and the kinetic arguments therefore support quenching in the amount of a factor of 5 or greater for FHEC layers. It remains unclear if desorption or further quenching occurs during the contact of FHEC with flowing PBS.

While a great number of factors could contribute to a reduction in the quantum yield of labels on adsorbed chains, we can rule out two possible contributions based on systematic studies. First, because we observe no adsorption of free fluorescein dye on silica particles[19] or flats,[17] label−surface interactions are not likely to contribute to reductions in quantum yield during adsorption. Second, calibration studies with mixtures of labeled and unlabeled PEO (per the datum in Figure 6A which represents the average of three trials) gave

lower coverages than those using only FPEO-labeled samples. If fluorophore−fluorophore interactions were responsible for a reduction in quantum yield, then the apparent coverage from the internal calibration with the mixture would have yielded a higher coverage from the layer with the lower labeling density. (The coverage was slightly reduced in the mixture sample because the unlabeled component was less degraded, and of higher molecular weight, and therefore preferred on the surface relative to the labeled component.) We also observed a proportionality between free FPEO concentration and initial rate of signal rise,[17] arguing against concentration quenching, at least during the initial stages of adsorption. There are many other factors potentially reducing quantum yield in adsorbed polymer layers, all of which are beyond the scope of this investigation. These include orientational and dynamic effects and chemical factors such as local hydrophobicity and the impact of the surface on local potential and ionic environment.[12] Finally, the different labeling topographies of FPEO and FHEC (chain ends vs random backbone tagging) may mean that quenching occurs to different extents and at different rates for the two molecules.

Conclusions

This work reexamined fundamental issues for the use of TIRF in quantitative studies of polymer adsorption and then compared TIRF-obtained isotherms to those on silica particles. We demonstrated that for layers which are stable to solvent washing, such as PEO, the best approach to an internal calibration is one where the calibration signal from free fluorophores is measured *in situ* during the adsorption run, a detail which eliminates inaccuracies due to variations in alignment and scattering between the calibration and adsorption runs. We also presented a new analysis method for angle-dependent data which is robust for experiments plagued by large amounts of light scattering. All internal calibrations relating the adsorbed layer signal to an adsorbed amount, relying on comparison to signal from a tracer fluid, are subject to inaccuracies induced by quantum yield changes during polymer adsorption. In this study, quantum yield reductions caused the apparent coverages measured by TIRF to be significantly lower than those on silica particles. Independent assessments for the FPEO coverages in this work suggest that for FPEO, a factor of 5 reduction in quantum yield occurs. Competition between high and low molecular weight chains in a polydisperse sample was also found to reduce the apparent coverage for samples labeled on a number-average basis, such as chain-end tagging.

For FPEO adsorption on silica, it was found that the isotherm shape measured by TIRF approached that found on silica particles, provided there was sufficient incubation time in the TIRF apparatus. In contrast, significant history dependence of FHEC adsorption was found. In these studies, coverage appeared to decrease as the layer continued to contact solvent. This process was attributed to either slow desorption or interfacial relaxations reducing the quantum yield within the layer. FHEC coverage appeared to decrease irreversibly and appeared not to recover when additional polymer solutions were introduced.

Acknowledgment. This work was made possible by the generous support of the Petroleum Research Foundation (23917-G7), the National Science Foundation (CTS 9209290), the Dana Foundation, and Lehigh's Chemical Engineering Department and Polymer Interfaces Center. Scanning angle capabilities were funded through Grants CTS 9202413 from NSF and RP-8019-02 from EPRI.

References and Notes

(1) Lok, B. K.; Cheng, Y. L.; Robertson, C. R. *J. Colloid Interface Sci.* **1983**, *91*, 87.
(2) Lok, B. K.; Cheng, Y. L.; Robertson, C. R. *J. Colloid Interface Sci.* **1983**, *91*, 104.
(3) Hlady, V.; Reinecke, D. R.; Andrade, J. D. *J. Colloid Interface Sci.* **1986**, *111*, 555.
(4) Hlady, V.; VanWagenen, R. A.; Andrade, J. D. In *Surface and Interfacial Aspects of Biomedical Polymers*; Andrade, J. D., Ed.; Plenum Press: New York, 1989; Vol. 2, p 81.
(5) Shibata, C. T.; Lenhoff, A. M. *J. Colloid Interface Sci.* **1992**, *148*, 469.
(6) Shibata, C. T.; Lenhoff, A. M. *J. Colloid Interface Sci.* **1992**, *148*, 485.
(7) Rondelez, F.; Ausserre, D.; Hervet, H. *Annu. Rev. Phys. Chem.* **1987**, *38*, 317.
(8) Caucheteux, I.; Hervet, H.; Jerome, R.; Rondelez, F. *J. Chem. Soc., Faraday Trans.* **1990**, *86*, 1369.
(9) Parsons, D.; Harrop, R.; Mahers, E. G. *Colloids Surf.* **1992**, *64*, 151.
(10) Kelly, M. S.; Santore, M. M. *Colloids Surf., A:* **1995**, *96*, 199−215.
(11) Santore, M. M.; Kelly, M. S.; Mubarykan, E.; Rebar, V. A. In *Surfactant Adsorption and Surface Solubilization*; ACS Symposium Series 615; Sharma, R., Ed.; American Chemical Society: Washington, DC, 1995; p 183.
(12) Rebar, V. A.; Santore, M. M. *J. Colloid Interface Sci.* **1996**, *178*, 29−41.
(13) Darst, S. A.; Robertson, C. R.; Berzofsky, J. A. *J. Colloid Interface Sci.* **1986**, *111*, 466.
(14) Robeson, J.; Tilton, R. *Langmuir* **1995**, *68*, 2145.
(15) Santore, M. M.; Rebar, V. A. In *Dynamics in Small Confining Systems II*; Drake, M., Troian, S. M., Klafter, J., Kopelman, R., Eds.; MRS Symp. Ser. 366; Materials Research Society: Pittsburgh, 1995.
(16) Rebar, v. A.; Santore, M. M. *Macromolecules*, following paper in this issue.
(17) Rebar, V. A. Ph.D. Dissertation, Lehigh University, 1995.
(18) Carlson, D. J.; Wiles, D. M. In *Encyclopedia of Polymer Science and Engineering*; John Wiley and Sons: New York, 1986; Vol. 14, p 603.
(19) Kelly, M.; Rebar, V. A.; Musikabhumma, A.; Santore, M. M. *Prog. Rep. Polym. Int. Center* **1992**, *2*, 15.
(20) Ausserre, D.; Hervet, H.; Rondelez, F. *Phys. Rev. Lett.* **1985**, *54*, 1948.
(21) Dijt, J. C.; Cohen Stuart, M. A.; Fleer, G. J. *Macromolecules* **1994**, *27*, 3207.
(22) Snowden, M. J.; Clegg, S. M.; Williams, P. A.; Robb, I. D. *J. Chem. Soc., Faraday Trans.* **1991**, *87*, 2201.
(23) Dijt, J. C.; Cohen Stuart, M. A.; Hofman, J. E.; Fleer, G. J. *Colloids Surf.* **1990**, *51*, 141.
(24) Killmann, E.; Maier, H.; Kaniut, P.; Gutling, N. *Colloids Surf.* **1985**, *15*, 261.
(25) Malmsten, M.; Linse, P.; Cosgrove, T. *Macromolecules* **1992**, *25*, 2474.
(26) Fleer, G. J.; Cohen Stuart, M. A.; Scheutjens, J. M. H. M.; Cosgrove, T.; Vincent, B. *Polymers at Interfaces*; Chapman and Hall: London, 1993.
(27) Fu, Z.; Santore, M. M., manuscript in preparation.

MA9512364